Broadband Phase Spectroscopy over Turbulent Air Paths

Fabrizio R. Giorgetta,[1,*] Gregory B. Rieker,[1] Esther Baumann,[1,†] William C. Swann,[1] Laura C. Sinclair,[1] Jon Kofler,[2] Ian Coddington,[1] and Nathan R. Newbury[1]
[1]National Institute of Standards and Technology, 325 Broadway, Boulder, Colorado 80305, USA
[2]National Oceanic and Atmospheric Administration, Boulder, Colorado 80305, USA
(Received 21 April 2015; published 1 September 2015)

Broadband atmospheric phase spectra are acquired with a phase-sensitive dual-frequency-comb spectrometer by implementing adaptive compensation for the strong decoherence from atmospheric turbulence. The compensation is possible due to the pistonlike behavior of turbulence across a single spatial-mode path combined with the intrinsic frequency stability and high sampling speed associated with dual-comb spectroscopy. The atmospheric phase spectrum is measured across 2 km of air at each of the 70 000 comb teeth spanning 233 cm^{-1} across hundreds of near-infrared rovibrational resonances of CO_2, CH_4, and H_2O with submilliradian uncertainty, corresponding to a 10^{-13} refractive index sensitivity. Trace gas concentrations extracted directly from the phase spectrum reach 0.7 ppm uncertainty, demonstrated here for CO_2. While conventional broadband spectroscopy only measures intensity absorption, this approach enables measurement of the full complex susceptibility even in practical open path sensing.

DOI: 10.1103/PhysRevLett.115.103901 PACS numbers: 42.62.Fi, 33.20.Vq, 42.68.Bz

Broadband phase spectra provide a rich source of information, representing half of the linear susceptibility, and thus could contribute significantly to sample analysis and sensing. Despite its fundamental importance, few instruments are capable of directly measuring broadband phase spectra. The derivative of the phase spectra can be acquired via tunable laser frequency-modulation spectroscopy [1], chirped laser dispersion spectroscopy [2], or frequency-comb Fourier transform spectroscopy [3]. Broadband phase spectra can be measured by dispersive Fourier transform spectroscopy [4]. Most conventional broadband spectrometers measure intensity for practical reasons; phase measurements require a stable optical path, which is challenging in the laboratory and fundamentally impossible in turbulent paths. Turbulence causes strong decoherence, for example, hundreds of radians of carrier phase noise and many picoseconds of pulse broadening over kilometer scale air paths. For this reason, no broadband atmospheric phase spectra have been acquired to date.

The phase coherence of dual-comb spectrometers does enable broadband phase measurements in the laboratory [5–11]. However, measurements of phase spectra over practical open paths would again appear impossible because of turbulence. Indeed, previous open-path dual-comb spectroscopy employed a non-phase-sensitive configuration where both combs were co-transmitted [12–14]. Because of simultaneous open path attenuation of both combs, this also removed the heterodyne gain that would otherwise be associated with this technique. Here, we show that turbulence phase noise does not in fact preclude the acquisition of broadband phase spectra over turbulent paths.

The elimination of turbulence phase noise in phase-sensitive dual-comb spectroscopy is possible due to its surprisingly simple behavior across a single-mode link combined with the intrinsic frequency stability and high sampling speed associated with dual-comb spectroscopy. Specifically, there are three important factors. First, the turbulence-induced phase noise has a measured power spectral density that falls off rapidly at higher Fourier frequencies. Therefore, the phase noise is effectively frozen over the time that the dual-comb spectrometer acquires a single spectrum, which is 2.3 ms here. Second, even under the moderate turbulence conditions explored here, we find the turbulence-induced phase noise follows a simple "piston"-like model where it can be described by a carrier phase shift combined with pulse timing noise. As a result, it is fully correlated across the comb spectrum. This strong correlation is likely valid only for a single spatial mode and is predicted to break down in the limit of very strong turbulence. Third, because dual-comb spectroscopy samples the medium at the precisely defined frequency of each comb tooth, we can use the dual-comb spectrometer data to quantify the turbulence piston phase noise very accurately, and then we can remove it equally accurately through a linear phase compensation. We thus acquire turbulence-compensated phase spectra with <5 mrad phase noise per tooth, corresponding to ~4.5 as of carrier timing noise, or a 10^5-fold suppression of the turbulence-induced phase noise. With higher-order baseline removal, appropriate for spectra with sharp molecular features, the phase noise becomes 0.6 mrad, corresponding to 0.6 as of relative timing noise or a refractive index change of $<10^{-13}$ over a 2 km path.

The setup for the phase-sensitive dual-comb spectrometer is illustrated in Fig. 1. Compared to Ref. [12], a single signal comb is transmitted over the turbulent open air path and received by a single-mode optical fiber. The signal and local oscillator (LO) fiber-based frequency combs are spectrally filtered to cover 6000 to 6250 cm^{-1}, overlapping

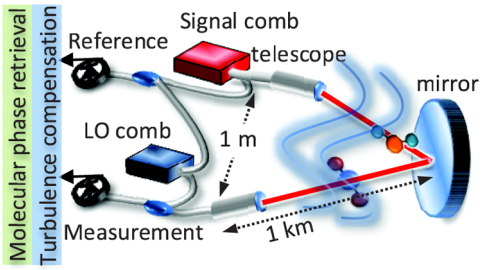

FIG. 1 (color online). Phase-sensitive, turbulence-compensated dual-comb spectrometer. The signal comb is transmitted across the 2 km turbulent path, recollected in a single-mode fiber, and heterodyned against the LO comb. The instantaneous turbulence phase noise is extracted from the data and used to self-compensate the measured complex spectrum, which is then normalized by the reference complex spectrum to retrieve the atmospheric molecular phase (and absorbance) spectrum. Gray, fiber; red, air path.

CH_4 and CO_2 bands. The signal comb is launched as a Gaussian beam with radius $w_0 = 2.5$ cm and power 1.65 mW. Steering mirrors at the launch and receive telescopes correct for slow beam wander, with the received power varying between 0 and ~ 10 μW due to turbulence. For our path length of $L = 2$ km, turbulence structure constant of $C_n^2 \sim 10^{-14}$ $\mathrm{m}^{-2/3}$, and a Gaussian beam, the Rytov variance is unity corresponding to moderate turbulence [15–17].

The signal and LO combs are phase locked to a stable optical reference such that their tooth frequencies are $\nu_m = \nu_0 + mf_r$ and $\nu_{\mathrm{LO},m} = \nu_0 + mf_{r,\mathrm{LO}}$, respectively, where ν_0 is a common anchor frequency and the repetition rates $f_{r(\mathrm{LO})} \sim 100$ MHz differ by $\Delta f_r = f_r - f_{r,\mathrm{LO}} \sim 440$ Hz [5–11,18,19]. The heterodyne signal is a series of interferograms, each of duration $1/\Delta f_r$, as the LO and signal pulses step through one another. Fourier transforming the interferogram yields a complex rf spectrum comprised of teeth with separation Δf_r, where each tooth has a one-to-one correspondence with the heterodyne beat between a signal and the LO comb tooth. This complex rf spectrum yields the amplitude and phase spectra through the atmosphere.

To understand the effects of turbulence on the measured phase spectrum, consider the field of the mth signal comb tooth $E_m(t, \rho, z) = E_m u(\nu_m, \rho, z) \exp(-i2\pi\nu_m t)$ propagating in the z direction with normalized single-mode spatial field u, radial coordinate ρ, and complex amplitude E_m. The extended Huygens-Fresnel integral [15–17] describes propagation over the turbulent path to the receiver aperture at $z = L$ where it is heterodyned against the corresponding LO comb tooth with complex amplitude $E_{m,\mathrm{LO}}$. The heterodyne signal is proportional to the spatial integral over the aperture between the signal and the LO field, $\iint u(\nu, \rho, L)u^*(\nu, \rho, 0)d^2\rho = T \exp[i\beta(\nu)L - \alpha(\nu)L/2 + \psi(t, \nu)]$, where T is the turbulence-free Gaussian-beam transmission (with negligible frequency dependence for a collimated beam), α is the atmospheric path absorbance, and ψ captures the effects of turbulence, spatially averaged over the aperture. β, our quantity of interest, includes both smooth phase-delay variations attributed to the air's dispersion and the sharper phase-delay variations associated with molecular resonances.

The complex heterodyne signal from one pair of teeth is then $\langle V_m(t)\rangle e^{im2\pi\Delta f_r t}$, where

$$\langle V_m(t)\rangle = a\{E_m E^*_{m,\mathrm{LO}}\} T \langle e^{\psi(t,\nu_m)}\rangle e^{-\alpha(\nu_m)L/2 + i\beta(\nu_m)L}. \quad (1)$$

The angle brackets indicate the average over the measurement time and a is the receiver gain. Normalization by the reference channel removes $a\{E_m E^*_{m,\mathrm{LO}}\}$ and then the natural logarithm gives the complex phase and amplitude spectrum $i\beta(\nu_m)L - \alpha(\nu_m)L/2$, except for the turbulence noise.

For a plane wave, turbulence theory gives the mean coherent field after propagation as $\langle \exp(\psi)\rangle \approx \exp(-2\pi^2 k_m^2 L \int_0^\infty \kappa\Phi(\kappa)d\kappa)$, where $\Phi(\kappa)$ is the turbulence spatial power spectral density (PSD), κ is the spatial frequency, and $k_m = 2\pi c^{-1}\nu_m$ [15–17]. For the often-used von Kármán PSD, $\langle \exp(\psi)\rangle \approx \exp(-0.39 C_n^2 k_m^2 L L_0^{5/3}) \approx \exp(-32000) \approx 0$, where $L_0 \sim 30$ m is the characteristic outer scale. In other words, turbulence leads to severe decoherence and zero signal.

However, there are several factors that allow us to compensate for the effects of turbulence. First, the decoherence is predominately driven by phase rather than amplitude variations. In fact, the exponential in the coherence decay is equivalent to $\langle \delta\theta^2\rangle = 0.5 {k_m}^2 L^2 \langle \delta n\rangle^2$, or the phase noise for a geometric ray from turbulence-driven variations in the refraction index δn [16]—in this picture the phase noise is due to pistonlike noise. Second, the dual-comb spectrometer acquires a complete phase spectrum with every interferogram, which is acquired in $1/\Delta f_r = 2.3$ ms. To estimate the accumulated phase noise over this short period, the Taylor frozen turbulence approximation is used to convert the spatial PSD to the temporal PSD as $S_\Phi(f) \equiv 2\pi U_t^{-1} \int_{-\infty}^{\infty} \Phi(\kappa_x, 2\pi f/U_t)d\kappa_x$, where $U_t = 1$ m/s is the transverse wind speed [17,20–22], giving $\langle \exp(\psi)\rangle_{1/\Delta f_r} \approx \exp[-2\pi^2 k_m^2 L \int_{\Delta f_r}^{\infty} S_\Phi(f)df] = -0.005 k_m^2 L C_n^2 (U_t/\Delta f_r)^{5/3} \approx \exp(-0.00005) \approx 1$ for our values, showing negligible decoherence. Therefore, we can simply measure the instantaneous carrier phase θ_c directly from each interferogram at a sample rate of Δf_r, then multiply the same raw data by $\exp(-i\theta_c)$ to remove its effect. As an empirically calculated value, θ_c includes any higher order phase noise beyond the piston approximation and varies by 1–2 rad/spectrum. This self-compensation effectively broadens the comb-tooth linewidth (resolution) but negligibly so (by $f^2 S_\Phi(f, U_t) \sim 15$ Hz in a Lorentzian approximation).

The dominant problem is not this carrier phase noise but rather the remaining differential phase noise across the several terahertz–wide comb that will mask the phase spectrum. In turbulence theory, this differential phase noise is captured by the (spatially averaged) two-frequency mutual coherence function $\Gamma(\Delta\nu = \nu_m - \nu_0)$, whose width

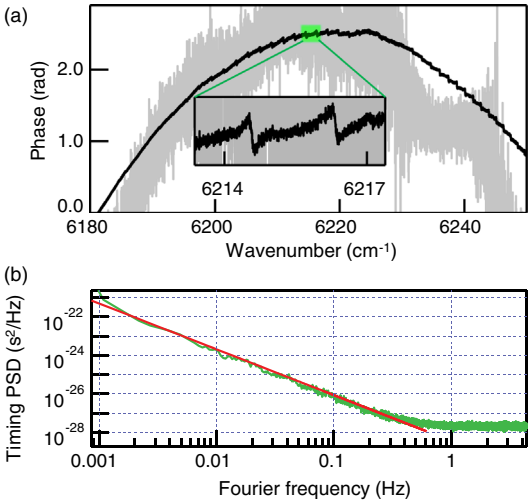

FIG. 2 (color online). (a) Phase spectrum averaged for 5 min without compensation (gray) and with turbulence compensation (black), where the molecular phase signatures are evident (see inset). (b) Power spectral density of the timing correction t_C (green) and a power-law scaling of $\sim f^{-2.4}$ (red).

is the coherence bandwidth and whose Fourier transform is the pulse broadening due to turbulence [15,23–28]. It is expanded as $\Gamma(\Delta\nu) = \Gamma_0(\Delta\nu)\Gamma_1(\Delta\nu)$. $\Gamma_0(\Delta\nu)$ reflects the pistonlike, line-of-sight turbulent optical path variations and leads to pulse-to-pulse timing noise while Γ_1 reflects higher order effects that lead to pulse spreading. Over a single spectrum acquisition, $\Gamma_0(\Delta\nu) \approx \exp[-2\pi^2 k_d^2 L \int_{\Delta f_r}^{\infty} S_\Phi(f) df] \approx \exp[-\Delta\nu^2/(10^{18}\ \mathrm{Hz})^2] \approx 1$, where $k_d = 2\pi c^{-1}\Delta\nu$. Therefore, the phase noise from $\Gamma_0(\Delta\nu)$ is removed in an analogous fashion to removing the carrier phase noise; we extract an instantaneous timing noise t_c directly from each interferogram, then multiply the same raw data by $\exp(-i2\pi\Delta\nu t_C)$ to remove its effect. This approach requires precisely defined comb tooth frequencies and an accurate estimate of t_c, both of which are possible by virtue of the frequency stability of the comb. More fundamentally, this approach assumes purely pistonlike noise or $\Gamma_1 = 1$. This assumption is violated by effects that cause two frequencies to sample different air paths, including multiple scattering from strong turbulence [15,23,24,26], the coupling of turbulence and Gaussian beam propagation outside the narrowband approximation [26,27], or a gradient in the atmospheric refraction index [28]. One would certainly expect it is violated in multimode propagation. In the extreme case of very strong turbulence, pulse spreading (Γ_1) will dominate over pulse-to-pulse timing wander (Γ_0) [15,23,26], prohibiting broadband phase spectroscopy. Despite extensive theoretical treatment, a general calculation of Γ_1 under moderate turbulence is challenging and there are no available experimental data. Therefore, it is not clear, *a priori*, whether a single timing correction is in fact adequate to cancel turbulence-driven phase noise. Empirically, we find here that it is.

We implement the turbulence phase compensation as follows. Each 225 000-point interferogram is digitized at 12 bits synchronously with $f_{r,\mathrm{LO}}$. Because of hardware limitations, we coherently average 50 interferograms before phase compensation [7,8,29], reducing the data burden while retaining full comb tooth resolution. This results in a modest SNR penalty that would be removed by real-time processing [30]. A 4096-point window centered around the interferogram centerburst is Fourier transformed to extract

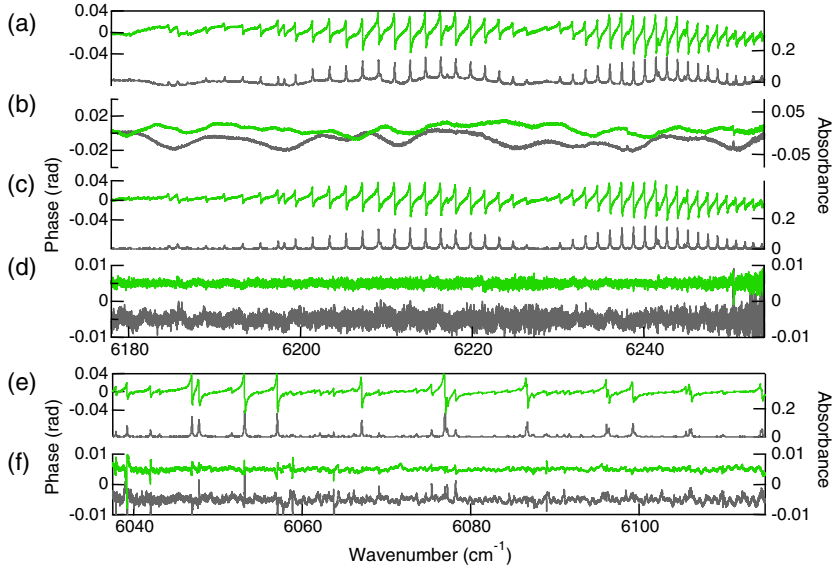

FIG. 3 (color online). (a) Phase $\beta(\nu)L$ (green, left axis) and absorbance $\alpha(\nu)L$ (gray, right axis) over an expanded 83 cm^{-1} window centered on the CO_2 band. Spectral data points are acquired at individual comb teeth spaced at 0.003 cm^{-1}. (b) Fit residuals for phase (5 mrad standard deviation) and absorbance. (c) Same spectra after a more aggressive piecewise baseline fit. (d) Corresponding fit residuals (offset) for phase (0.6 mrad standard deviation) and absorbance (1.3×10^{-3} standard deviation). (e) Similar data to (c) but for a spectral window centered to include CH_4 and water resonances. (f) Corresponding fit residuals (offset).

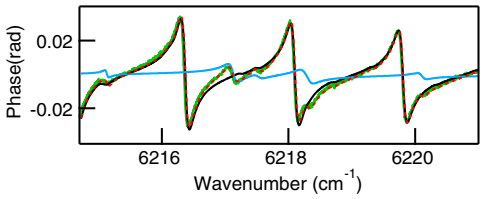

FIG. 4 (color online). Expanded view of the phase spectrum (green) and fit (dashed red) along with the individual contributions from CO_2 (black) and water (blue).

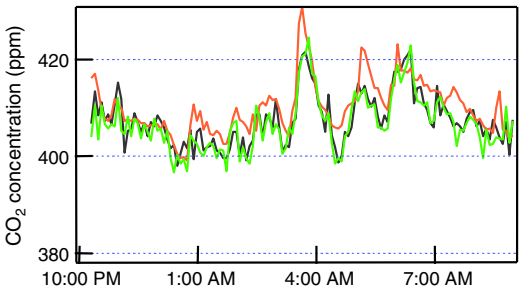

FIG. 5 (color online). Extracted CO_2 concentration from the phase (green) and amplitude (gray) spectra as well as from a nearby calibrated point sensor (orange).

the smoothed phase spectrum, which is subtracted from the $t = 0$ phase spectrum. This phase difference is fit to a line to find an offset θ_c and slope t_C, which are then used for the phase compensation. Figure 2(a) shows a phase spectrum acquired with and without turbulence phase compensation over a 5 min acquisition. (The parabolic phase profile originates from dispersion of the additional 3.2 m of fiber to the reference channel and the 2-km air path.) Figure 2(b) shows the PSD of t_C extracted over an ~11 h time period, from which we estimate $C_n^2 \sim 3 \times 10^{-14}$ $m^{-2/3}$ [22]; note that the overall shape follows a power law of $f^{-2.4}$ rather than the theoretical $f^{-8/3}$ and does not exhibit the expected low frequency cutoff at $\sim U_t/L_0$, in agreement with previous turbulence phase measurements [22]. Turbulence will also cause signal intensity variations mainly on time scales longer than Δf_r^{-1} (see Fig. S1 in Ref. [12]). If the return signal drops below ~300 nW, the phase unwrapping algorithm fails and these interferograms are discarded. Here, we discard ~3% of the interferograms.

The signal comb is spectrally shaped to cover two absorption bands, the $CO_2$30013←00001 combination band and a portion of the CH_4 tetradecad. Figure 3(a) shows the complex spectrum $i\beta(\nu)L - \alpha(\nu)L/2$ over the 83 cm^{-1} spectral window containing the CO_2 band sampled at each of the 25 000 comb teeth separated by 0.003 cm^{-1}, acquired over ~11 h (including 344 430 individual spectra), demonstrating that long-time coherent averaging is possible. For these spectra, the parabolic phase evident in Fig. 2(a) is removed via a cubic polynomial; alternatively, a short (meter-scale) free-space reference path could eliminate the reference path fiber, allowing direct access to, and interrogation of, the air dispersion. The phase spectrum in Fig. 3(a) shows multiple molecular resonances. A resonance with 10% absorbance will exhibit sharp phase excursions of $\sim \pm 5$ mrad, corresponding to an index change of $\pm 7 \times 10^{-13}$, with tails decaying as ν^{-2}.

Just as with molecular absorbance, the molecular phase signature scales linearly with concentration. Therefore, we can extract the gas concentration directly from the phase spectra alone by fitting it to a model based on the HITRAN 2008 [31] database, the complex Voigt line shape, and the measured air pressure and temperature. (The Voigt profile for the phase fit is given by the imaginary part of the complex error function.) The fit uses a single concentration for each isotopologue, whose spectrum is the sum over all known resonances. Figure 4 shows an expanded window that includes a CO_2 and H_2O resonance, demonstrating the high fit quality despite strong overlapping phase signatures. As shown in Fig. 3(b), the fit residuals over the spectrum have an $\sim \pm 15$ mrad wander, which we attribute to phase variations between the signal and reference spectra.

The ~0.15 cm^{-1}-wide collision-broadened resonances typical of small molecules allow us to apply a more aggressive baseline fit. The spectrum of Fig. 3(a) is split into 6.3 cm^{-1}-wide windows that overlap by 0.13 cm^{-1}. Each window is fit by a spectral model summed with a 7th order polynomial. These polynomials are concatenated to form a baseline, which is subtracted to yield Fig. 3(c), whose fit residuals are 0.6 mrad, as shown in Fig. 3(d). Figure 3(e) shows the similar spectrum for the CH_4 tetradecad window. The residuals across the CH_4 spectral band sometimes exhibit structure near molecular resonances that we attribute to incorrect spectral line parameters, line shape models, and line mixing effects.

Figure 5 compares the CO_2 concentration extracted independently from the fit to the phase and absorbance spectra at 5-min intervals over the 11 h period. The two agree to ± 2.3 ppm at 5-min intervals and 0.7 ppm on average. The concentration time dependence shows true fluctuations in the path-averaged CO_2 concentration, as verified by a co-located point sensor [12]. The sub-1% agreement with the point sensor is coincidental as we expect no better than a few percent agreement given the different sampling volumes and CO_2 line strength uncertainty [12].

In conclusion, we present the first broadband measurements of atmospheric phase spectra, possible through phase-sensitive dual-comb spectroscopy. The milliradian sensitivity is comparable to the $\sim 10^{-3}$ sensitivity routinely achieved with direct absorption spectroscopy and is realized on a comb tooth-by-tooth basis despite turbulence. Direct phase detection avoids the bandwidth limitations and systematics associated with a Kramers-Kronig transformation of the absorption spectrum. The SNR here is comparable to the open-path measurements of Ref. [12], where both near infrared combs were transmitted in a phase-insensitive configuration. However, the phase sensitive configuration uses heterodyne detection against a local oscillator comb so that it can reach the shot-noise limit with high path attenuation, which should be important for future

measurements in the mid- or long-wave infrared where the combs might be weaker and detectors noisier [8,9,32,33]. In general, this approach expands the capabilities of broadband spectroscopy to include phase as well as absorbance, which should enable better sample characterization, improved trace gas detection, and high-resolution refractive index data to support high-resolution ranging or timing applications.

We acknowledge funding from NIST and the DARPA SCOUT program, and helpful comments from G. Ycas, A. Klose, G. W. Truong, and M. Dowell.

*fabrizio.giorgetta@nist.gov
†baumann@nist.gov

[1] G. C. Bjorklund, Frequency-modulation spectroscopy: a new method for measuring weak absorptions and dispersions, Opt. Lett. **5**, 15 (1980).
[2] M. Nikodem and G. Wysocki, Molecular dispersion spectroscopy—new capabilities in laser chemical sensing, Ann. N.Y. Acad. Sci. **1260**, 101 (2012).
[3] J. Mandon, G. Guelachvili,, and N. Picqué, Fourier transform spectroscopy with a laser frequency comb, Nat. Photonics **3**, 99 (2009).
[4] J. R. Birch, Dispersive Fourier transform spectroscopy, Microchim. Acta **93**, 105 (1987).
[5] I. Coddington, W. C. Swann, and N. R. Newbury, Coherent multiheterodyne spectroscopy using stabilized optical frequency combs, Phys. Rev. Lett. **100**, 013902 (2008).
[6] M. Brehm, A. Schliesser, and F. Keilmann, Spectroscopic near-field microscopy using frequency combs in the mid-infrared, Opt. Express **14**, 11222 (2006).
[7] A. M. Zolot, F. R. Giorgetta, E. Baumann, J. W. Nicholson, W. C. Swann, I. Coddington, and N. R. Newbury, Direct-comb molecular spectroscopy with accurate, resolved comb teeth over 43 THz, Opt. Lett. **37**, 638 (2012).
[8] E. Baumann, F. R. Giorgetta, W. C. Swann, A. M. Zolot, I. Coddington, and N. R. Newbury, Spectroscopy of the methane ν_3 band with an accurate midinfrared coherent dual-comb spectrometer, Phys. Rev. A **84**, 062513 (2011).
[9] Y. Jin, S. M. Cristescu, F. J. M. Harren, and J. Mandon, Two-crystal mid-infrared optical parametric oscillator for absorption and dispersion dual-comb spectroscopy, Opt. Lett. **39**, 3270 (2014).
[10] A. A. Lanin, A. A. Voronin, A. B. Fedotov, and A. M. Zheltikov, Time-domain spectroscopy in the mid-infrared, Sci. Rep. **4** 6670 (2014).
[11] G. Taurand, P. Giaccari, J.-D. Deschénes, and J. Genest, Time-domain optical reflectometry measurements using a frequency comb interferometer, Appl. Opt. **49**, 4413 (2010).
[12] G. B. Rieker, F. R. Giorgetta, W. C. Swann, J. Kofler, A. M. Zolot, L. C. Sinclair, E. Baumann, C. Cromer, G. Petron, C. Sweeney, P. P. Tans, I. Coddington, and N. R. Newbury, Frequency-comb-based remote sensing of greenhouse gases over kilometer air paths, Optica **1**, 290 (2014).
[13] A. Schliesser, M. Brehm, F. Keilmann, and D. van der Weide, Frequency-comb infrared spectrometer for rapid, remote chemical sensing, Opt. Express **13**, 9029 (2005).
[14] S. Boudreau, S. Levasseur, C. Perilla, S. Roy, and J. Genest, Chemical detection with hyperspectral lidar using dual frequency combs, Opt. Express **21**, 7411 (2013).
[15] L. C. Andrews and R. L. Phillips, *Laser Beam Propagation through Random Media*, 2nd ed. (SPIE, Bellingham, WA, 2005).
[16] R. L. Fante, Electromagnetic beam propagation in turbulent media, Proc. IEEE **63**, 1669 (1975).
[17] A. Ishimaru, *Wave Propagation and Scattering in Random Media* (Academic Press, New York, 1978).
[18] B. Bernhardt, A. Ozawa, P. Jacquet, M. Jacquey, Y. Kobayashi, T. Udem, R. Holzwarth, G. Guelachvili, T. W. Hänsch, and N. Picqué, Cavity-enhanced dual-comb spectroscopy, Nat. Photonics **4**, 55 (2010).
[19] F. Zhu, T. Mohamed, J. Strohaber, A. A. Kolomenskii, T. Udem, and H. A. Schuessler, Real-time dual frequency comb spectroscopy in the near infrared, Appl. Phys. Lett. **102**, 121116 (2013).
[20] G. I. Taylor, The spectrum of turbulence, Proc. R. Soc. A **164**, 476 (1938).
[21] J. M. Conan, G. Rousset, and P.-Y. Madec, Wave-front temporal spectra in high-resolution imaging through turbulence, J. Opt. Soc. Am. A **12**, 1559 (1995).
[22] L. C. Sinclair, F. R. Giorgetta, W. C. Swann, E. Baumann, I. Coddington, and N. R. Newbury, Optical phase noise from atmospheric fluctuations and its impact on optical time-frequency transfer, Phys. Rev. A **89**, 023805 (2014).
[23] C. H. Liu and K. C. Yeh, Pulse spreading and wandering in random media, Radio Sci. **14**, 925 (1979).
[24] I. Sreenivasiah and A. Ishimaru, Beam wave two-frequency mutual-coherence function and pulse propagation in random media: an analytic solution, Appl. Opt. **18**, 1613 (1979).
[25] C. Y. Young, L. C. Andrews, and A. Ishimaru, Time-of-arrival fluctuations of a space-time Gaussian pulse in weak optical turbulence: an analytic solution, Appl. Opt. **37**, 7655 (1998).
[26] R. L. Fante, Two-position, two-frequency mutual-coherence function in turbulence, J. Opt. Soc. Am. **71**, 1446 (1981).
[27] C. Y. Young, A. Ishimaru, and L. C. Andrews, Two-frequency mutual coherence function of a Gaussian beam pulse in weak optical turbulence: an analytic solution, Appl. Opt. **35**, 6522(1996).
[28] C. S. Gardner, Effects of random path fluctuations on the accuracy of laser ranging systems, Appl. Opt. **15**, 2539 (1976).
[29] I. Coddington, W. C. Swann, and N. R. Newbury, Coherent dual-comb spectroscopy at high signal-to-noise ratio, Phys. Rev. A **82**, 043817 (2010).
[30] J. Roy, J.-D. Deschénes, S. Potvin, and J. Genest, Continuous real-time correction and averaging for frequency comb interferometry, Opt. Express **20**, 21932 (2012).
[31] L. S. Rothman *et al.*, The HITRAN 2008 molecular spectroscopic database, J. Quant. Spectrosc. Radiat. Transfer **110**, 533 (2009).
[32] A. Schliesser, N. Picqué, and T. W. Hänsch, Mid-infrared frequency combs, Nat. Photonics **6**, 440 (2012).
[33] C. Y. Wang, T. Herr, P. Del'Haye, A. Schliesser, J. Hofer, R. Holzwarth, T. W. Hänsch, N. Picqué, and T. J. Kippenberg, Mid-infrared optical frequency combs at 2.5 μm based on crystalline microresonators, Nat. Commun. **4**, 1345 (2013).